Computers and Mathematics with Applications 59 (2010) 3053–3065

Contents lists available at ScienceDirect

Computers and Mathematics with Applications

journal homepage: www.elsevier.com/locate/camwa

Effect of heating location and size on mixed convection in lid-driven cavities

V. Sivakumar [a], S. Sivasankaran [b,*], P. Prakash [c], Jinho Lee [d]

[a] Department of Mathematics, Nandha Engineering College, Erode 638 052, India
[b] Department of Mathematics, University College, Sungkyunkwan University, Suwon 440-746, South Korea
[c] Department of Mathematics, Periyar University, Salem 636 011, India
[d] School of Mechanical Engineering, Yonsei University, Seoul 120-749, South Korea

ARTICLE INFO

Article history:
Received 2 April 2009
Received in revised form 27 December 2009
Accepted 17 February 2010

Keywords:
Convection
Lid-driven cavity
Partial heating
Size of heating portion

ABSTRACT

A numerical study is performed to analyze the mixed convection heat transfer and fluid flow in lid-driven cavities with different lengths of the heating portion and different locations of it. The left wall has been heated fully or partially to a higher temperature, whereas the right wall is maintained at a lower temperature. Three different lengths of the heating portion and three different locations of it are used along the hot wall. The remaining portions of the left wall, and the top and the bottom walls of the cavity are insulated. The finite volume method is used to discretize the governing equations which are then solved iteratively. The velocities and pressure are coupled by the SIMPLE algorithm. Results are presented graphically in the form of streamlines, isotherms and velocity profiles. It is concluded that the heat transfer rate is enhanced on reducing the heating portion and when the portion is at middle or top of the hot wall of the cavity.

1. Introduction

Mixed convection flow and heat transfer is one of the major problems studied in the thermo-fluids area. It has possible applications in many engineering, technological and natural processes. This includes food processing, crystal growth, electronic cooling, oil extraction, solar collectors and thermo-hydraulics of nuclear reactors. Many investigations have been conducted on lid-driven cavity flow and heat transfer during the past three decades using experimental or numerical methods by several investigators. Mohamad and Viskanta [1] investigated the effects of a sliding lid on the fluid flow and thermal structures in a shallow lid-driven cavity. They found that the maximum local heat transfer rate occurs at the starting area of the sliding lid and decreases along the sliding lid. Chenak et al. [2] studied mixed convection and conduction heat transfer in open cavities. They showed that heat transfer across the cavity is enhanced when the cavity aspect ratio is increased. Prasad and Koseff [3] investigated combined forced and natural convection in a lid-driven cavity experimentally. Chamkha [4] investigated the problem of unsteady laminar combined convection flow and heat transfer of an electrically conducting and heat generating or absorbing fluid in a vertical lid-driven cavity in the presence of a uniform magnetic field. He found that the presence of the internal heat generation effect is found to decrease the average Nusselt number significantly for aiding flow and to increase it for opposing flow. How and Hsu [5] examined transient mixed convection in a partially divided enclosure. They revealed that the time to reach the steady state depends strongly on the configuration of the divider.

* Corresponding author.
E-mail address: sd.siva@yahoo.com (S. Sivasankaran).

0898-1221/$ – see front matter © 2010 Elsevier Ltd. All rights reserved.
doi:10.1016/j.camwa.2010.02.025

Nomenclature

c_p	specific heat, J/(kg K)
g	gravitational acceleration, m/s^2
Gr	Grashof number
k	thermal conductivity, W/(m K)
L	cavity length, m
L_H	heater length, m
$\underline{Nu}$	local Nusselt number
$\overline{Nu}$	average Nusselt number
P	pressure, Pa
Pr	Prandtl number
Re	Reynolds number
T	temperature, °C
ΔT	temperature difference, $T_h - T_c$
t	time, s
u, v	velocity components, m/s
U, V	dimensionless velocities
U_0	lid velocity, m/s
W	cavity width, m
x, y	Cartesian coordinates, m
X, Y	dimensionless Cartesian coordinates

Greek symbols

α	thermal diffusivity, m^2/s
β	coefficient of thermal expansion of fluid, K^{-1}
θ	dimensionless temperature
ρ	density of the fluid, kg/m^3
μ	dynamic viscosity, Pa s
ν	kinematic viscosity, m^2/s
ψ	stream function, m^2/s
τ	dimensionless time

Subscripts

c	cold wall
h	hot wall
H	heater

Zhang [6] examined numerical simulation of a two-dimensional square driven cavity using fourth-order compact finite difference schemes. He compared his computed solutions up to $Re = 7500$ with the benchmark solutions obtained by other researchers. Hossain and Gorla [7] numerically investigated the effect of viscous dissipation on mixed convection flow in a rectangular enclosure. They drew the conclusion that the heat transfer rate from the top heated surface is increased on increasing the Eckert number and Reynolds number. Amiri et al. [8] provided numerical simulation of combined thermal and mass transport in a square lid-driven cavity. Their results demonstrated that the heat and mass transfer rates inside the cavity are enhanced for low values of Richardson numbers. A numerical study on laminar mixed convection in shallow driven cavities with a hot moving lid on top that are cooled from the bottom has been carried out by Sharif [9]. He observed that average Nusselt number increases slightly with the cavity inclination angle for the forced convection dominated case while it increases much more rapidly with inclination angle for the natural convection dominated case. Ji et al. [10] performed a numerical and experimental study on transient mixed convection in a lid-driven enclosure. They showed that the temperature field exhibits weak fluctuating behavior at early times in the mid and upper portions of the cavity.

Convection in a two-dimensional square cavity with partially heated walls has been an important topic because of its applications such as in electronic equipment cooling, solar energy collectors and nuclear reactors. Kuhn and Oosthuizen [11] numerically investigated unsteady natural convection in a partially heated rectangular cavity. Their results showed that the heat transfer is affected by the position of the heated element unless the heater is very close to a horizontal wall. Yucel and Turkoglu [12] studied natural convection in a rectangular enclosure with partial heating and cooling. They found that the mean Nusselt number decreases with increasing heater size for a given cooler size and that the Nusselt number increases on increasing the cooler size for a given heater size. Oztop [13] made a numerical study on combined convection heat transfer in a partially heated lid-driven enclosure. He found that the location of the heater is the most effective parameter on combined

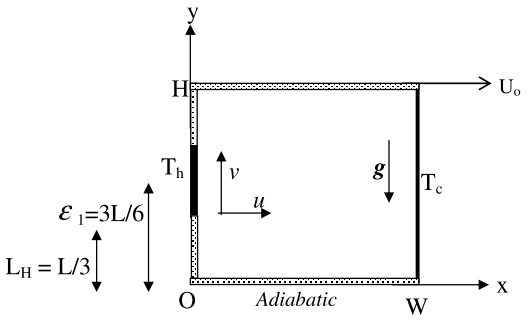

Fig. 1a. Schematic diagram of the physical configuration and the coordinate system.

convection flow and temperature field. He concluded that heat transfer is enhanced when the heater is located on the left vertical wall. Chen and Chen [14] numerically investigated laminar, steady, two-dimensional natural convection flows in a square enclosure partially heated on the left and bottom walls. They revealed that the heat transfer rate is gradually increased by increasing the length of the heat source segment.

Kandaswamy et al. [15] made a numerical study on buoyancy-driven convection in an enclosure with partially thermally active vertical walls. Their results illustrated that heat transfer rate is increased when the heating location is at middle of the hot wall. Nithyadevi et al. [16,17] numerically studied the natural convection in a square cavity with partially active vertical walls. They found that the heat transfer rate is enhanced when the heating location is at the middle of the hot wall. Ghasemi and Aminossadati [18] carried out a numerical study on mixed convection in a partially heated square cavity. In this study, they kept the right wall at low temperature and move vertically either a constant velocity or with a sinusoidal oscillation. The results indicated that the direction and magnitude of the sliding wall velocity affect the heat transfer rate. At low Richardson numbers, the average heat transfer rate for a cavity with an oscillating wall is lower than that for a cavity with a constant velocity wall.

In most of the studies found in the literature, vertical walls are considered to be isothermal in mixed convection flow and heat transfer in enclosures. However, in many engineering applications the heater and cooler play an important role in the fluid flow and heat transfer, particularly for electronic equipment cooling. In order to understand the effect of heater size and locations on mixed convection, in the present study we examine the heat transfer and fluid flow for different sizes of the heating portion and different locations of it in a lid-driven cavity.

2. Mathematical formulation

Consider unsteady, laminar, incompressible combined convective flow and heat transfer in a two-dimensional square cavity of size L filled with air. The top and bottom walls of the cavity are insulated. The left wall is either fully or partially heated to temperature T_h while the right wall is maintained at a temperature T_c such that $T_h > T_c$. Three different lengths L_H of the heating portion and three different locations of it are used along the hot wall. The remaining portions are adiabatic while partially heating the left wall. The top wall of the cavity is allowed to move in its own plane at a constant speed U_0. The physical model and the coordinate system considered in the investigation are shown in Fig. 1a. The thermo-physical properties of the fluid are assumed to be constant, except in the buoyancy term. The Boussinesq approximation is valid. It is further assumed that viscous dissipation is neglected in the study.

$$\frac{\partial u}{\partial x} + \frac{\partial v}{\partial y} = 0 \tag{1}$$

$$\frac{\partial u}{\partial t} + u\frac{\partial u}{\partial x} + v\frac{\partial u}{\partial y} = -\frac{1}{\rho_0}\frac{\partial p}{\partial x} + \nu\left(\frac{\partial^2 u}{\partial x^2} + \frac{\partial^2 u}{\partial y^2}\right) \tag{2}$$

$$\frac{\partial v}{\partial t} + u\frac{\partial v}{\partial x} + v\frac{\partial v}{\partial y} = -\frac{1}{\rho_0}\frac{\partial p}{\partial y} + \nu\left(\frac{\partial^2 v}{\partial x^2} + \frac{\partial^2 v}{\partial y^2}\right) + g\beta(T - T_c) \tag{3}$$

$$\frac{\partial T}{\partial t} + u\frac{\partial T}{\partial x} + v\frac{\partial T}{\partial y} = \frac{k}{\rho_0 c_p}\left(\frac{\partial^2 T}{\partial x^2} + \frac{\partial^2 T}{\partial y^2}\right) \tag{4}$$

where t, u, v, p, T, x and y are the time, fluid velocity components in the x- and y-directions, pressure, temperature and the coordinate directions, respectively. The parameters β, k, ν, ρ_0, c_p and g are the fluid volumetric thermal expansion coefficient, thermal conductivity, kinematic viscosity, fluid density, the specific heat, and acceleration due to gravity, respectively.

Table 1
Comparison of average Nusselt number with available literature values for lid-driven cavity.

Gr	*Re*					
	400			1000		
	Present work	Reference [9]	Difference (%)	Present work	Reference [9]	Difference (%)
10^2	4.09	4.5	−9.11	6.48	6.55	−1.07
10^4	3.85	3.82	0.78	6.47	6.50	−0.46
10^6	1.10	1.17	−5.98	1.66	1.81	−8.28

The initial and boundary conditions for the problem can be written as follows:

$$\left.\begin{array}{lll}
\text{For } t=0: & u=v=0 & T=0, \quad 0\le(x,y)\le L \\
\text{For } t>0: & u=v=0 & \dfrac{\partial T}{\partial y}=0 \quad y=0 \\
& u=U_0;\ v=0 & \dfrac{\partial T}{\partial y}=0 \quad y=L \\
& u=v=0 & T=T_c \quad x=L \\
& u=v=0 & x=0. \\
\text{Case 1: (Increasing heater length from bottom)} & & \\
T=T_h & x=0,\ 0\le y\le \varepsilon_1+L/6 & \\
\dfrac{\partial T}{\partial x}=0 & x=0,\ \varepsilon_1+L/6\le y\le L & \\
\text{Case 2: (Increasing heater length from top)} & & \\
T=T_h & x=0,\ \varepsilon_1-L/6\le y\le L & \\
\dfrac{\partial T}{\partial x}=0 & x=0,\ 0\le y\le \varepsilon_1-L/6 & \\
\text{Case 3: (Heater placement)} & & \\
T=T_h & x=0,\ \varepsilon_1-L/6\le y\le \varepsilon_1+L/6 & \\
\dfrac{\partial T}{\partial x}=0 & x=0,\ 0\le y\le \varepsilon_1-L/6,\ \varepsilon_1+L/6\le y\le L &
\end{array}\right\} \tag{5}$$

where $\varepsilon_1 = L/6$, $3L/6$ and $5L/6$ denotes the distance of the center of the heating portion from the bottom of the cavity. In case 1, the normalized length, L_H, of the heat source is varied as $L/3$, $2L/3$, L of the cavity height, extending from the bottom left corner. In case 2, the heat source L_H, is varied as $L/3$, $2L/3$, L of the cavity height, increasing from the top left corner. In case 3, L_H is kept constant at $L/3$ but the placement is varied at the bottom, middle, and top of the left wall so that ε_1 is $L/6$, $3L/6$, $5L/6$ from the lower left corner. However, the heater length $L_H = L/3$ at the bottom in case 1 and the placement of heater when $\varepsilon_1 = 1/6$ at the bottom in case 3 are the same. Similarly, the heater length $L_H = L/3$ at the top in case 2 and the placement of heater when $\varepsilon_1 = 5L/6$ at the top in case 3 are the same. Thus, there are three cases with six configurations.

It is convenient to non-dimensionalize Eq. (1) through (5) using the following dimensionless variables:

$$X=\frac{x}{L}, \quad Y=\frac{y}{L}, \quad U=\frac{u}{U_0}, \quad V=\frac{v}{U_0}, \quad \theta=\frac{T-T_C}{T_H-T_C}, \quad \tau=\frac{tU_0}{L}, \quad \varepsilon_2=\frac{\varepsilon_1}{L} \quad \text{and} \quad P=\frac{p}{\rho U_o^2}. \tag{6}$$

The previous governing equations result in the following dimensionless equations:

$$\frac{\partial U}{\partial X}+\frac{\partial V}{\partial Y}=0 \tag{7}$$

$$\frac{\partial U}{\partial \tau}+U\frac{\partial U}{\partial X}+V\frac{\partial U}{\partial Y}=-\frac{\partial P}{\partial X}+\frac{1}{Re}\left(\frac{\partial^2 U}{\partial X^2}+\frac{\partial^2 U}{\partial Y^2}\right) \tag{8}$$

$$\frac{\partial V}{\partial \tau}+U\frac{\partial V}{\partial X}+V\frac{\partial V}{\partial Y}=-\frac{\partial P}{\partial Y}+\frac{1}{Re}\left(\frac{\partial^2 V}{\partial X^2}+\frac{\partial^2 V}{\partial Y^2}\right)+\frac{Gr}{Re^2}\theta \tag{9}$$

$$\frac{\partial \theta}{\partial \tau}+U\frac{\partial \theta}{\partial X}+V\frac{\partial \theta}{\partial Y}=\frac{1}{Pr\,Re}\left(\frac{\partial^2 \theta}{\partial X^2}+\frac{\partial^2 \theta}{\partial Y^2}\right) \tag{10}$$

where the Reynolds number $Re = U_0 L/\nu$, the Grashof number $Gr = g\beta\Delta T L^3/\nu^2$, the Prandtl number $Pr = \nu/\alpha$, and the thermal diffusivity $\alpha = k/\rho C_p$.

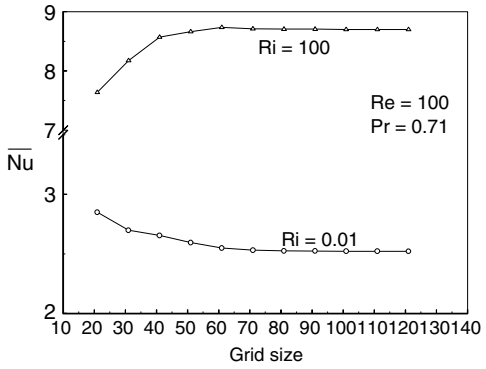

Fig. 1b. Grid independent test.

The dimensionless initial and boundary conditions of the problem under consideration can be written as

$$
\begin{aligned}
&\text{For } \tau = 0: \quad U = V = 0 \qquad \theta = 0 \qquad 0 \le (X, Y) \le 1\\
&\text{For } \tau > 0: \quad U = V = 0; \qquad \frac{\partial \theta}{\partial Y} = 0 \quad Y = 0\\
&\qquad\qquad\quad U = 1; V = 0; \qquad \frac{\partial \theta}{\partial Y} = 0 \quad Y = 1\\
&\qquad\qquad\quad U = V = 0 \qquad \theta = 0 \qquad X = 1\\
&\qquad\qquad\quad U = V = 0 \qquad\qquad\quad X = 0\\
&\text{Case 1:} \quad \theta = 1 \qquad X = 0, 0 \le Y \le \varepsilon_2 + 1/6\\
&\qquad\quad \frac{\partial \theta}{\partial X} = 0 \quad X = 0, \varepsilon_2 + 1/6 \le Y \le 1\\
&\text{Case 2:} \quad \theta = 1 \qquad X = 0, \varepsilon_2 - 1/6 \le y \le 1\\
&\qquad\quad \frac{\partial \theta}{\partial X} = 0 \quad X = 0, 0 \le y \le \varepsilon_2 - 1/6\\
&\text{Case 3:} \quad \theta = 1 \qquad X = 0, \varepsilon_2 - 1/6 \le Y \le \varepsilon_2 + 1/6\\
&\qquad\quad \frac{\partial \theta}{\partial X} = 0 \quad X = 0, 0 \le Y \le \varepsilon_2 - 1/6, \varepsilon_2 + 1/6 \le Y \le 1
\end{aligned}
\tag{11}
$$

where $\varepsilon_2 = 1/6$, 3/6 and 5/6.

The stream function is defined in the usual way as $U = \frac{\partial \psi}{\partial Y}$ and $V = -\frac{\partial \psi}{\partial X}$. It is taken that $\psi = 0$ at all walls of the cavity. The local Nusselt number and average Nusselt number at the hot wall of the cavity are expressed as $Nu = -\left(\frac{\partial \theta}{\partial X}\right)_{x=0}$ and $\overline{Nu} = \frac{1}{L_H}\int_0^{L_H} Nu \, dY$, respectively, where L_H is the length of the heating portion.

3. Method of solution

The governing equations (7)–(10) together with the boundary conditions (11) are discretized using the finite volume method [19]. The QUICK scheme [20] is used for the convective terms and the central difference scheme is used for the diffusive terms. An implicit scheme is used for time marching. The velocities and pressure are coupled by the SIMPLE algorithm [19]. An iterative process solves each variable obtained from the resulting set of discretized equations. The process is repeated until the following convergence criterion is satisfied: $\left|\frac{\Phi_{n+1}(i,j) - \Phi_n(i,j)}{\Phi_{n+1}(i,j)}\right| \le 10^{-6}$ for each variable. In order to determine the proper grid size for this study, a grid independence test is conducted for $Ri = 0.01$ and 100 in a square cavity. A uniform grid is chosen in both X- and Y-directions. It is found that an 81×81 grid is sufficiently fine to ensure a grid independent solution; see Fig. 1b. The agreement between the present computational result and that of Sharif [9] is seen to be good with a maximum discrepancy of about 9.11, which is shown in Table 1. The present code is also validated against the result of Chamkha [4]. This is shown in Fig. 1c.

4. Result and discussion

The combined free and forced convection heat transfer and fluid flow for different lengths of the heating portion and different locations of it in a lid-driven cavity is numerically investigated. The working fluid is chosen as air with Prandtl number $Pr = 0.71$. The Reynolds number is taken as 10^2 and 10^3 and the Grashof number is varied from 10^2 to 10^6. The Richardson number provides a measure for the importance of the natural convection relative to the forced convection effect.

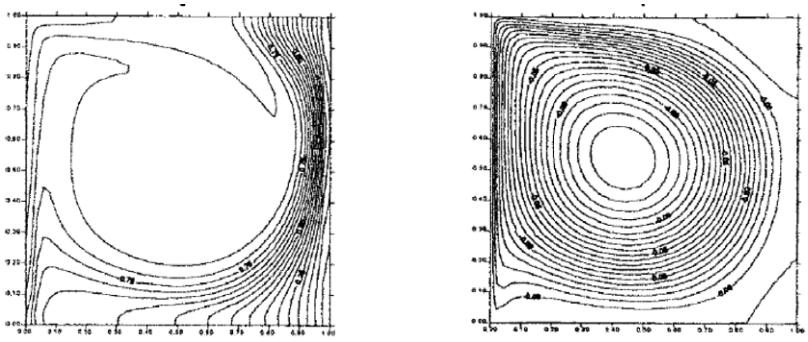

(i) Chamkha [4]

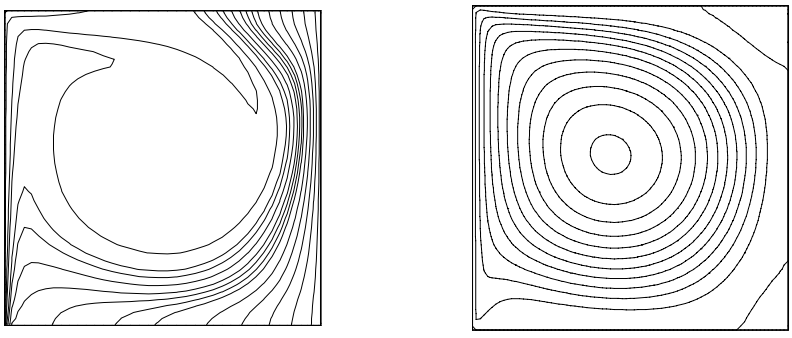

(ii) Present study

Fig. 1c. Comparison of the isotherms and streamlines for $Gr = 100$, $Re = 1000$, $Pr = 0.71$ with the work of Chamkha [4].

The Richardson number is varied from 0.01 to 100. The effects of three different lengths ($L_H = 1/3, 2/3$ and 1) of the heating portion and three different locations ($\varepsilon_2 = 1/6, 3/6$ and $5/6$) of it on the heat transfer and fluid flow inside the two-dimensional square lid-driven cavity are investigated numerically.

4.1. Effect of the size of the heating portion

Fig. 2(a)–(f) show typical temperature contours for different Richardson numbers ($Ri = 0.01, 1.0, 100$) and different lengths of heating portion ($L_H = 1/3, 2/3, 1$) with $\varepsilon_2 = 1/6, 2/6, 3/6$ and $5/6$, respectively. The isotherms are distributed over the entire cavity when the Richardson number is small in Fig. 2(a), i.e. forced convection dominates. On increasing the Richardson number to $Ri = 100$, thin boundary layers are formed at both the left bottom of the hot wall and the top of the cold wall, as natural convection dominates. The same temperature effect is seen except near to the hot wall in Fig. 2(b) for different Richardson numbers as occurred in Fig. 2(a) for different lengths of heating portions. It is also found that the isotherms show vertical temperature stratification for $Ri = 100$. When $L_H = 2/3$ and $\varepsilon_2 = 5/6$, the isotherms are distributed over the whole cavity for forced and mixed convection regimes. However, thermal stratification in the core region disappears when $Ri = 100$. This is clearly seen from Fig. 2(c). The heat distribution inside the cavity is very poor when reducing the heating portion size to $L_H = 1/3$, which is clearly seen from the isotherm patterns in Fig. 2(d)–(f).

Fluid flow is displayed in the form of streamlines for different Richardson numbers and for different lengths of the heating portion ($Ri = 0.01, 1.0, 100$) in Fig. 3. Fig. 3(a) shows that there is a primary circulating eddy in the above half of the cavity generated by the movement of the top wall for $Ri = 0.01$. Buoyancy force does not play an important role when Ri is less than unity. Since the shear force dominates the buoyancy force, the core region of the circulating eddy inside the cavity is near to the top of the cavity. Neither forced convection nor natural convection dominates at $Ri = 1.0$, and the core region of the eddy moves to the center of the cavity. The eddy occupies the whole cavity for the natural convection dominated case, $Ri = 100$, and the eddy is elongated horizontally. The circulation rate of the eddy is slightly increased when the Richardson number is increased. Fig. 3(b) and (c) show that there is no considerable change in the flow field on reducing the heating length at $Ri = 0.01$ and $Ri = 1.0$. But, in the case of natural convection dominated flow, the flow field is altered depending on heating location. The area of the core region is decreased and flow speed is increased considerably when the heating portion is reduced to $L_H = 2/3$ and $L_H = 1/3$; see Fig. 3(b) & (d).

4.2. Effect of the position of the heating portion

The influence of different locations of the heating portion for different Richardson numbers, $Ri = 0.01, 1.0$ and 100 is displayed in Fig. 2(d)–(f). Fig. 2(d) exhibits that when forced convection dominates ($Ri = 0.01$), the isotherms are crowded

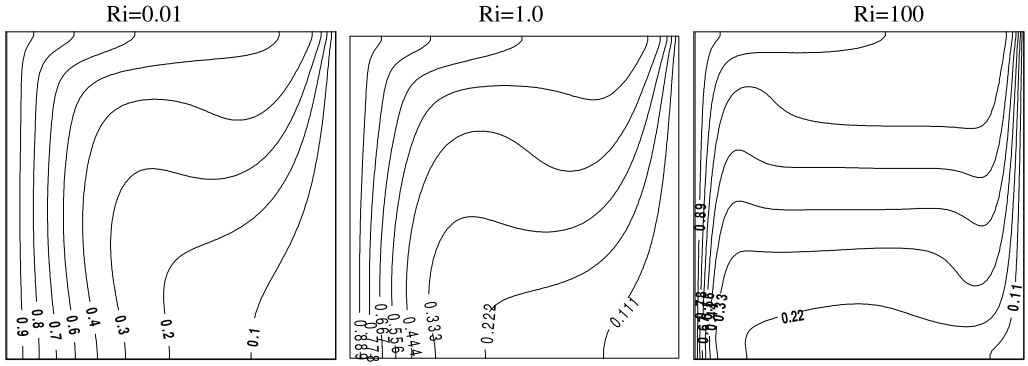

(a) $L_H = 1, \varepsilon_2 = 3/6$.

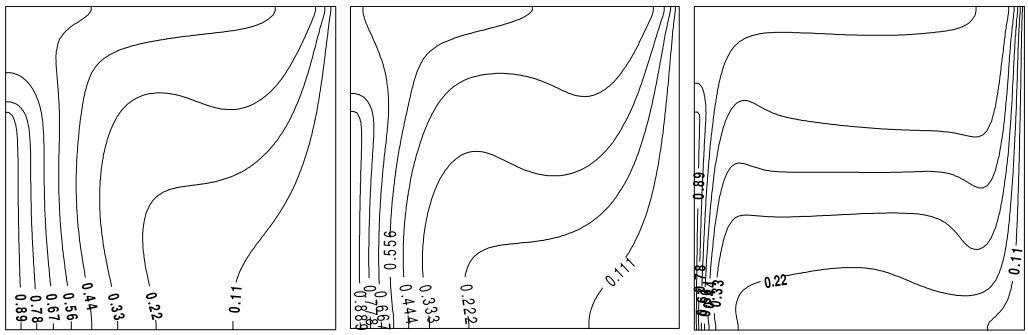

(b) $L_H = 2/3, \varepsilon_2 = 2/6$.

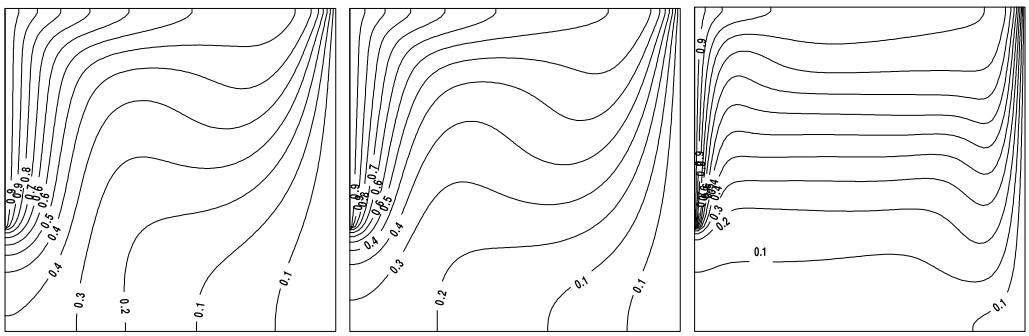

(c) $L_H = 2/3, \varepsilon_2 = 5/6$.

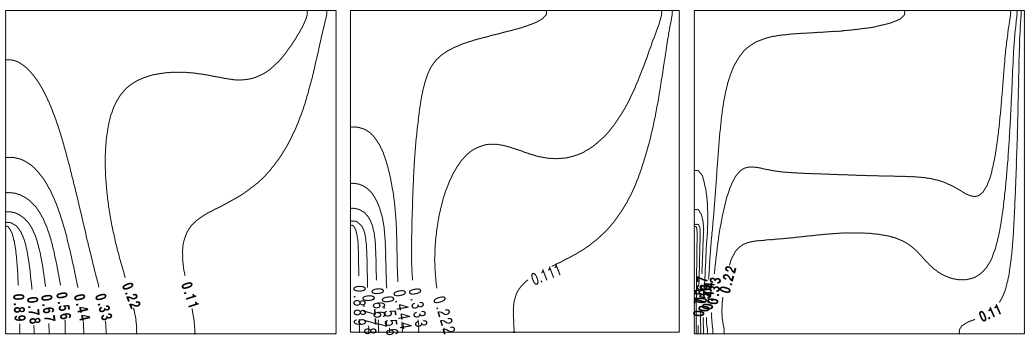

(d) $L_H = 1/3, \varepsilon_2 = 1/6$.

Fig. 2. Isotherms for different Richardson numbers and different heating locations.

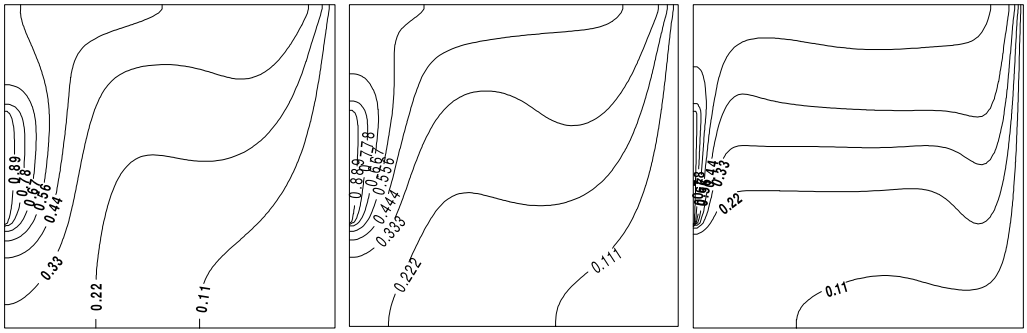

(e) $L_H = 1/3, \varepsilon_2 = 3/6$.

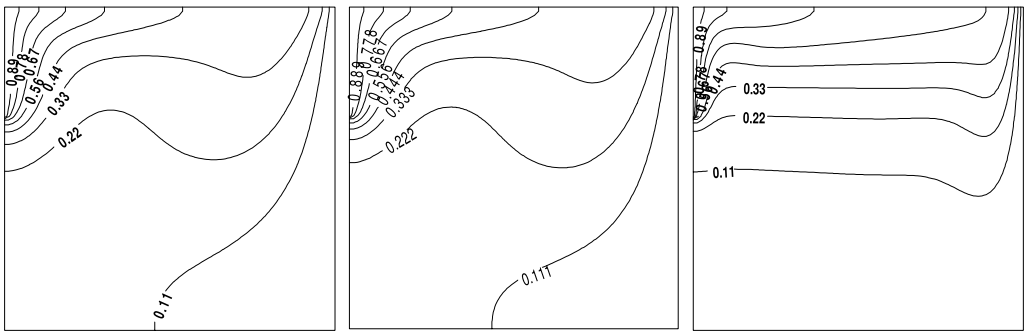

(f) $L_H = 1/3, \varepsilon_2 = 5/6$.

Fig. 2. (*continued*)

at the left bottom of the cavity because the heating portion is kept at the bottom of the cavity. On increasing the Richardson number to $Ri = 1.0$, the isotherms move towards the heating portion. Thin boundary layers are formed at both the left bottom of the hot wall and the top of the cold wall as natural convection dominates on increasing the Richardson number to $Ri = 100$. This is evidence for a good heat transfer rate. Fig. 2(e) shows the occurrence of the same temperature effect except near to the heating portion. By changing the location of the heating portion to the top of the hot wall, transfer of heat is by conduction in the lower half of the cavity for a given Richardson number.

Fluid flow for different locations of the heating portion for different Richarson numbers is displayed in Fig. 3(d)–(f). Fig. 3(d) shows that there is a primary circulating eddy in the upper half of the cavity generated by the movement of top wall for $Ri = 0.01$. As the shear force dominates, the core region of the circulating eddy is near to the moving lid of the cavity. It moves to the centre of the cavity and occupies the entire cavity in the mixed convection regime, i.e., $Ri = 1.0$. It is observed that the eddy is stretched out in the natural convection dominant case ($Ri = 100$). The same flow patterns occur as in Fig. 3(d) for all convections that are presented in Fig. 3(e). It is very interesting to see that the flow speed is decreased on changing the location of the heating portion from the bottom to the top for $Ri = 100$. That is, natural convection becomes stronger when the heater is at the bottom of the wall. There is no considerable change in the absolute value of the stream function on changing the location of the heating portion from the bottom to the top for $Ri = 0.01$.

4.3. Effect on the heat transfer rate

Fig. 4(a)–(b) display the local Nusselt numbers for different Richardson numbers and different lengths of the heating portion. In Fig. 4(a), a high heat transfer rate is observed near to the adiabatic portion of the hot wall because the buoyancy force is boosted up in the presence of some unheated space above the heating portion. But such behavior is not found in the fully heated wall. On increasing the Richardson number, there is a considerable increment in the local Nusselt number. Similar behavior of the local Nusselt number is observed when $Re = 1000$ in Fig. 4(b). Fig. 5(a)–(b) present the local Nusselt numbers for different Richardson numbers for different locations of the heating portion. Fig. 5(a) shows that a high heat transfer rate occurs near to the adiabatic portion of the hot wall. Since the buoyancy force is improved in the presence of some unheated space above the heating portion, the same performance is not initiated when the heating portion is located at the top of the hot wall. There is a significant increment in local Nusselt number on increasing the Richardson number. Comparable behavior of the local Nusselt number is observed when $Re = 1000$ in Fig. 5(b).

The time history of the average Nusselt number for different Richardson number is displayed in Fig. 6. In the beginning, the average Nusselt number is suddenly decreased and a steady state is reached after some time. When the Richardson number is increased, the heat transfer rate increases constantly. The steady state is reached more quickly in the natural

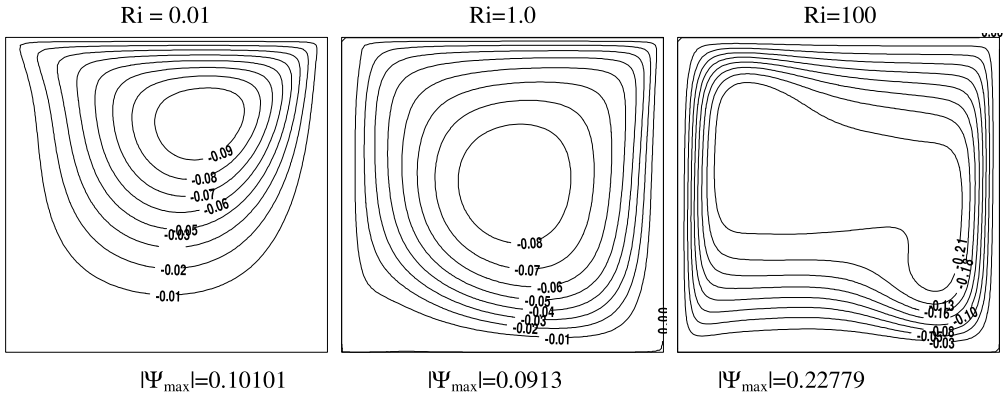

(a) $L_H = 1, \varepsilon_2 = 3/6$.

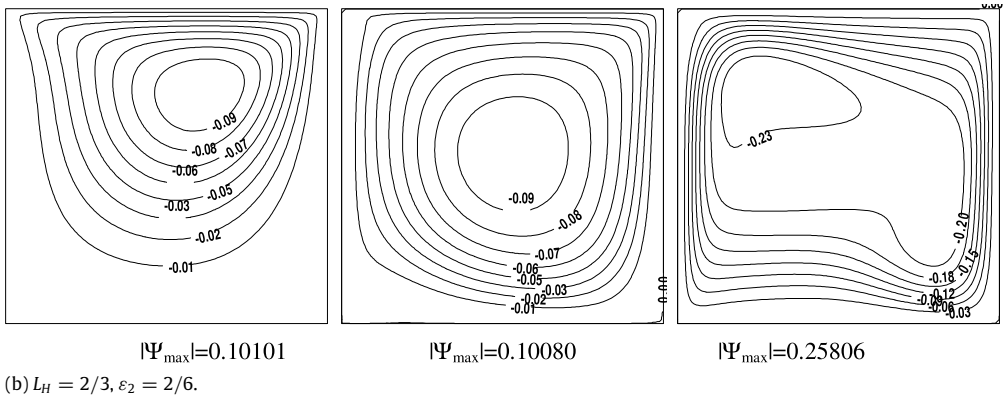

(b) $L_H = 2/3, \varepsilon_2 = 2/6$.

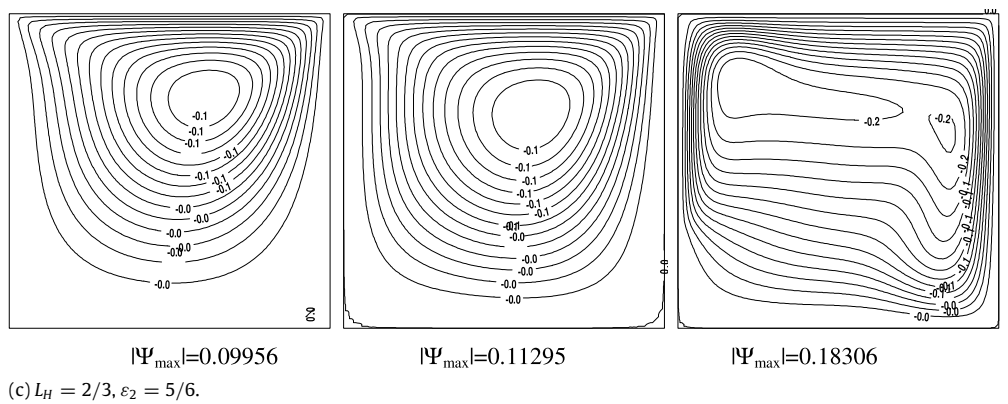

(c) $L_H = 2/3, \varepsilon_2 = 5/6$.

Fig. 3. Streamlines for different Richardson numbers and different heating locations.

convection case than in the forced convection case. The time to reach steady state is very high for $Ri = 1$, that is, the mixed convection regime. The effect of average Nusselt number versus time is displayed in Fig. 7 for different locations and different lengths of the heating portion at $R = 1.0$. In Fig. 7(a), the heat transfer rate is increased when the length of the heating portion is reduced. The time to reach steady state is reduced on increasing the length of the heating portion. It is interesting to see that the heat transfer is higher for the heating portion being in the middle of the hot wall than for the other two locations. Fig. 7(b) shows the effect of heat transfer rate for different places of heating. The heat transfer rate is enhanced when the heating portion is at the middle of the hot wall of the cavity. The time to reach steady state is increased when the heating portion is at the top of the hot wall. Fig. 8(a)–(b) presents the average Nusselt number versus Richardson number for different lengths of the heating portion. It is observed that the heat transfer rate is increased when the Richardson number is increased and the length of the heating portion is reduced for $Ri = 100$; see Fig. 8(a). It is also observed that the heat transfer rate is very high when the heating portion is reduced and it is placed at the bottom of the hot wall for $Ri = 10^3$;

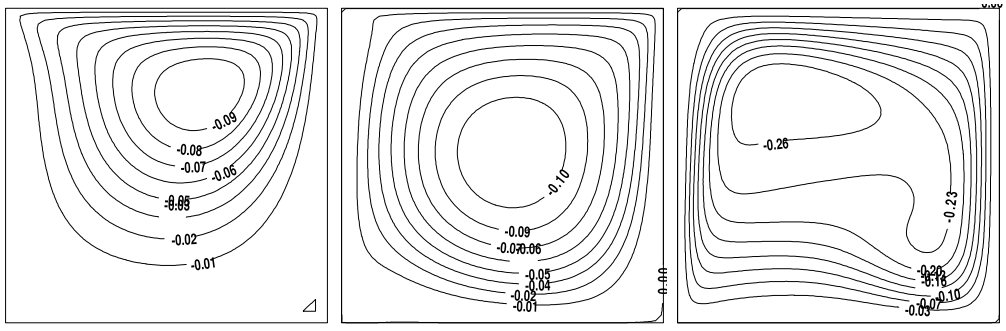

$|\Psi_{max}|$=0.10101 $|\Psi_{max}|$=0.1090 $|\Psi_{max}|$=0.28209

(d) $L_H = 1/3, \varepsilon_2 = 1/6$.

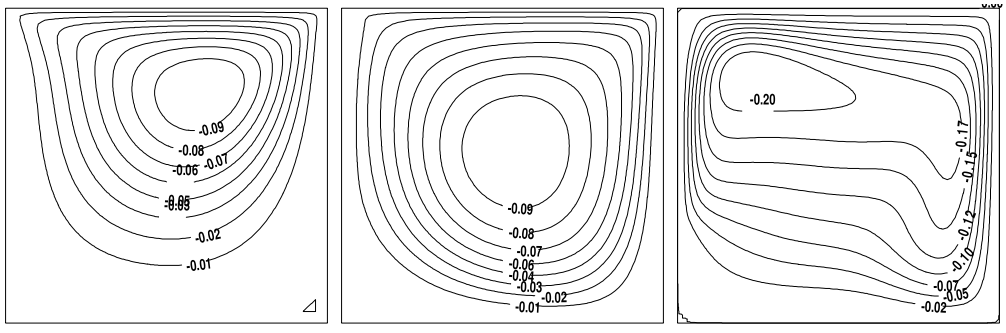

$|\Psi_{max}|$=0.10103 $|\Psi_{max}|$=0.09868 $|\Psi_{max}|$=0.2150

(e) $L_H = 1/3, \varepsilon_2 = 3/6$.

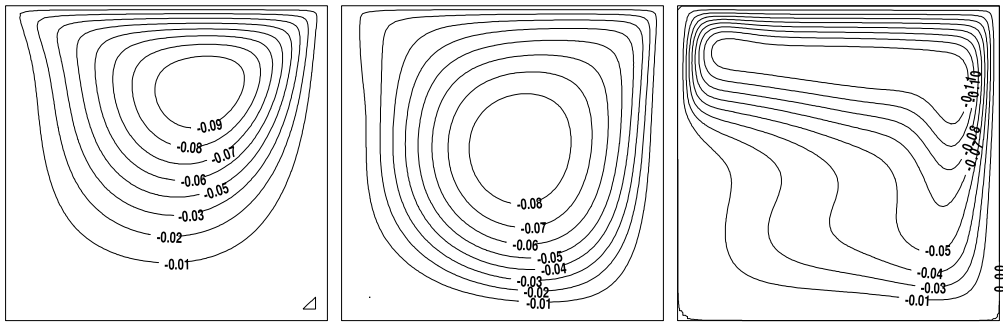

$|\Psi_{max}|$=0.10088 $|\Psi_{max}|$=0.09331 $|\Psi_{max}|$=0.12002

(f) $L_H = 1/3, \varepsilon_2 = 5/6$.

Fig. 3. (*continued*)

this is clearly seen in Fig. 8(b). It is noted here that a high heat transfer rate occurs in both cases ($Re = 10^2$ & $Re = 10^3$) on keeping the length of the heating portion at $L_H = 1/3$ and placing it at $\varepsilon_2 = 1/6$. On comparing these two graphs, it is found that a better heat transfer rate is obtained by reducing the heating portion length.

In order to find the effect on the heat transfer rate of the location of the heating portion, the average Nusselt number against Richardson numbers for different locations of the heating portion are depicted in Fig. 9(a)–(b). Both figures show that the heat transfer rate is increased when the Richardson number is increased. There are fluctuations with Richardson number when locating the heating portion from the bottom to the top on hot wall; see Fig. 9(a). The heat transfer rate is enhanced on placing the heating portion at the top of the hot wall for $Ri < 1$, whereas the heat transfer rate is enhanced on placing the heating portion at the middle of the hot wall for $Ri \geq 1$. That is, in the case of forced convection the top heating location provides better heat transfer rate, and the middle heating location gives better heat transfer in the case of natural convection. However, the opposite behavior is observed for $Ri = 10^3$ in Fig. 9(b). That is, in the case of forced convection, the middle heating location provides better heat transfer rate, and the top heating location gives better heat transfer in the case

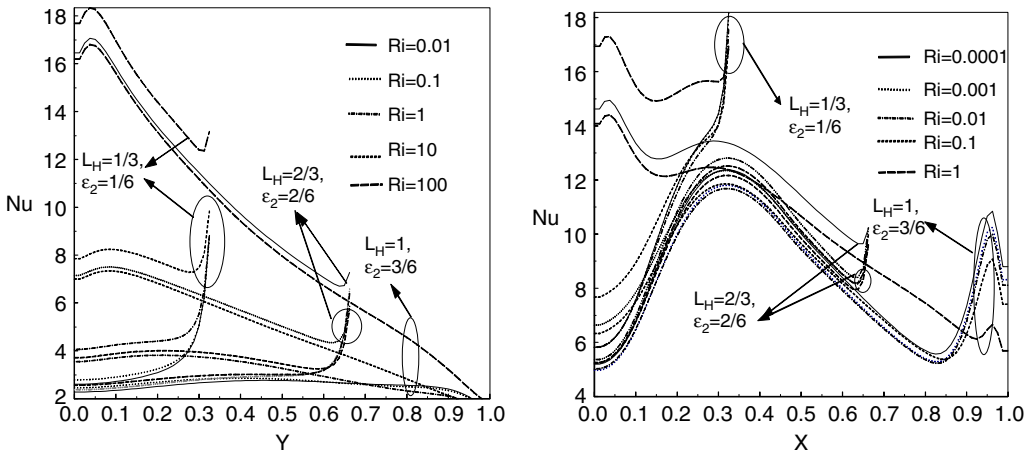

(a) $Re = 10^2$. (b) $Re = 10^3$.

Fig. 4. Local Nusselt number for different Ri and L_H with $\varepsilon_2 = 3/6, 2/6$ and $1/6$.

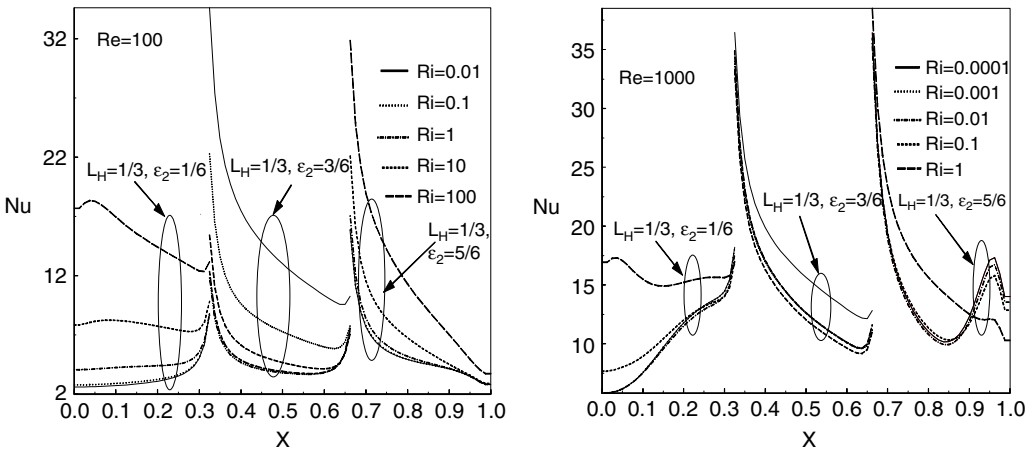

(a) $Re = 10^2$. (b) $Re = 10^3$.

Fig. 5. Local Nusselt number for different Ri and ε_2 with $L_H = 1, 2/3$ and $1/3$.

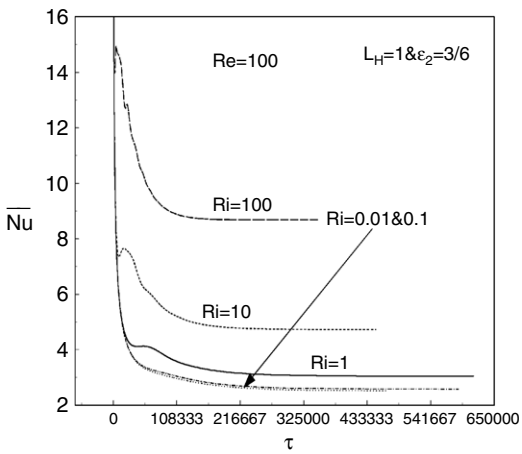

Fig. 6. Time history of average Nu for different Ri with $Re = 100$, $L_H = 1$ and $\varepsilon_2 = 3/6$.

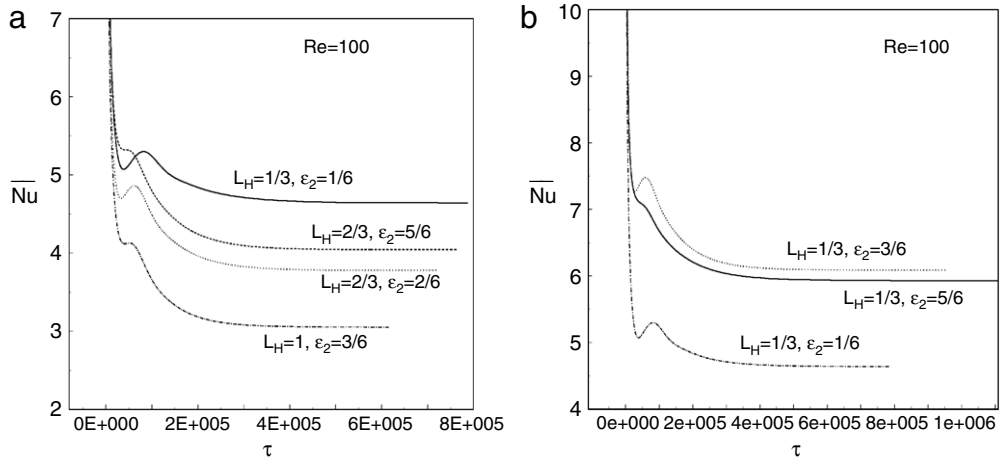

Fig. 7. Time history of average *Nu* for different L_H and ε_2 with $Re = 100$ and $Ri = 1$.

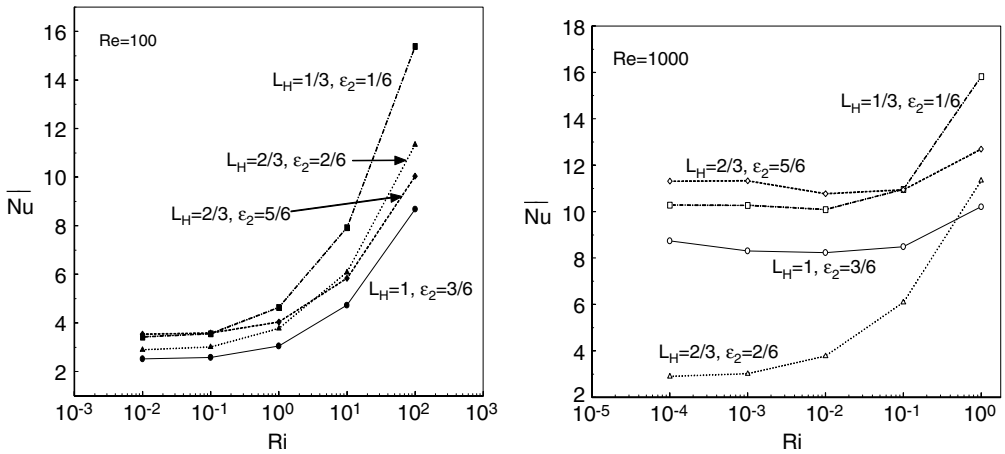

(a) $Re = 10^2$. (b) $Re = 10^3$.

Fig. 8. Average Nusselt number versus *Ri* for $L_H = 1, 2/3, 1/3$ with $\varepsilon_2 = 1/6, 2/6, 3/6$, $Re = 10^2$ and 10^3.

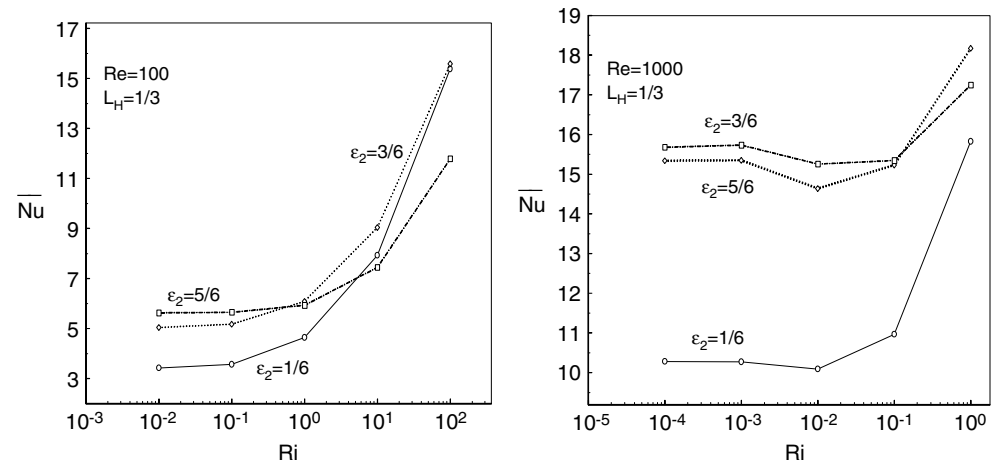

(a) $Re = 10^2$. (b) $Re = 10^3$.

Fig. 9. Average Nusselt number versus *Ri* for $\varepsilon_2 = 1/6, 2/6, 3/6$ with $L_H = 1/3$, $Re = 10^2$ and 10^3.

of natural convection. It is observed from Fig. 9(a) and (b) that the heat transfer rate is enhanced when the heating location is at the middle or top of the hot wall depending on the Reynolds number. Comparing Figs. 8 and 9, it is also observed that the heat transfer rate is enhanced on reducing the heating portion and while the portion is at the middle or top of the hot wall of the cavity.

5. Conclusion

A numerical study has been performed to analyze mixed convection heat transfer and fluid flow in a lid-driven cavity with different lengths of the heating portion and different locations of it. There is no considerable change in the flow field on reducing the heating portion length at $Ri = 0.01$ and $Ri = 1.0$. But, in the case of $Ri = 100$ (natural convection dominated flow), the flow field depends strongly on the heating location. A steady state is reached more quickly in the natural convection case than in the forced convection case. The time to reach steady state is very high for the mixed convection regime. It is found that a better heat transfer rate is obtained on reducing the heating portion length in the hot wall of a differentially heated cavity. It is observed that the heat transfer rate is enhanced when the heating location is at the middle or top of the hot wall depending on the Reynolds number. From the above two results, it is concluded that the heat transfer rate is enhanced on reducing the length of the heating portion and when the portion is at the middle or top of the hot wall of the cavity.

References

[1] A.A. Mohamad, R. Viskanta, Flow and heat transfer in a lid-driven cavity filled with a stably stratified fluid, Appl. Math. Modelling 19 (1995) 465–472.
[2] A.K. Chenak, M. Mbaye, P. Vasseur, E. Bilgen, Mixed convection and conduction heat transfer in open cavities, Int. J. Heat Mass Transfer 30 (1995) 229–235.
[3] A.K. Prasad, J.R. Koseff, Combined forced and natural convection heat transfer in a deep lid driven cavity flow, Int. J. Heat Fluid Flow 17 (1996) 460–467.
[4] A.J. Chamkha, Hydromagnetic combined convection flow in a vertical lid-driven cavity with internal heat generation or absorption, Numer. Heat Transfer Part A 41 (2002) 529–546.
[5] S.P. How, T.H. Hsu, Transient mixed in a partially divided enclosure, Comput. Math. Appl. 36 (1998) 95–115.
[6] J. Zhang, Numerical simulation of 2D square driven cavity using fourth-order compact finite difference schemes, Comput. Math. Appl. 45 (2003) 43–52.
[7] M.A. Hossian, R.S.R. Gorla, Effect of viscous dissipation on mixed convection flow of water near its density maximum in a rectangular enclosure with isothermal wall, Internat. J. Numer. Methods Heat Fluid Flow 16 (2006) 5–17.
[8] A. Amiri, M. Khanafer, I. Pop, Numerical simulation of combined thermal and mass transport in a square lid-cavity, Int. J. Thermal Sci. 46 (2007) 662–671.
[9] M.A.R. Sharif, Laminar mixed convection in shallow inclined driven cavities with hot moving lid on top and cooled from bottom, Appl. Thermal Eng. 27 (2007) 1036–1042.
[10] T.H. Ji, S.Y. Kim, J.M. Hyun, Transient mixed convection in an enclosure driven by a sliding lid, Int. J. Heat Mass Transfer 43 (2007) 629–638.
[11] D. Kuhn, P.H. Oosthuizen, Unsteady natural convection in a partially heated rectangular cavity, J. Heat Transfer 109 (1987) 798–801.
[12] N. Yucel, H. Turkoglu, Natural convection in rectangular enclosures with partial heating and cooling, Heat Mass Transfer 29 (1994) 471–478.
[13] F. Oztop, Combined convection heat transfer in porous lid-driven enclosure due to heater with fine length, Int. Commun. Heat Mass Transfer 33 (2006) 772–779.
[14] T.H. Chen, L.Y. Chen, Study of buoyancy-induced flows subjected to partially heated sources on the left and bottom walls in a square enclosure, Int. J. Thermal Sci. 46 (2007) 1219–1231.
[15] P. Kandaswamy, S. Sivasankaran, N. Nithyadevi, Buoyancy-driven convection of water near its density maximum with partially active vertical walls, Int. J. Heat Mass Transfer 50 (2007) 942–948.
[16] N. Nithyadevi, P. Kandaswamy, S. Sivasankaran, Natural convection in a square cavity with partially active vertical walls: Time periodic boundary condition, Math. Probl. Eng. 2006 (2006) 1–16.
[17] N. Nithyadevi, S. Sivasankaran, P. Kandaswamy, Buoyancy-driven convection of water near its density maximum with time periodic partially active vertical walls, Meccanica 42 (2007) 503–510.
[18] B. Ghasemi, S.M. Aminossadati, Comparison of mixed convection in a square cavity with an oscillating versus a constant velocity wall, Numer. Heat Transfer Part A 54 (2008) 726–743.
[19] S.V. Patankar, Numerical Heat Transfer and Fluid Flow, Hemisphere, Washington DC, 1980.
[20] H.K. Versteeg, W. Malalasekara, An introduction to computational fluid dynamics: The finite volume method, Longman Scientific & Technical, England, 1995.